Title

Morphology-controlled transformation of Cu@Au core-shell nanowires into thermally stable Cu3Au intermetallic nanowires

Journal

Nano Research, 13(9)

ISSN

1998-0124

Authors

Niu, Zhiqiang
Chen, Shouping
Yu, Yi
et al.

Publication Date

2020-09-01

DOI

10.1007/s12274-020-2900-z

Peer reviewed

Morphology-controlled transformation of Cu@Au core−shell nanowires into thermally stable Cu_3Au intermetallic nanowires

Zhiqiang Niu[1,3,§], Shouping Chen[2,4,§], Yi Yu[5], Teng Lei[1], Ahmad Dehestani[3], Kerstin Schierle-Arndt[3], and Peidong Yang[1,2,3,4,6] (✉)

[1] *Department of Chemistry, University of California, Berkeley, California 94720, USA*
[2] *Department of Materials Science and Engineering, University of California, Berkeley, California 94720, USA*
[3] *California Research Alliance (CARA), BASF Corporation, Berkeley, California 94720, USA*
[4] *Materials Sciences Division, Lawrence Berkeley National Laboratory, Berkeley, California 94720, USA*
[5] *School of Physical Science and Technology, ShanghaiTech University, Shanghai 201210, China*
[6] *Kavli Energy NanoScience Institute, Berkeley, California 94720, USA*
[§] *Zhiqiang Niu and Shouping Chen contributed equally to this work.*

ABSTRACT Multimetallic nanowires with long-range atomic ordering hold the promise of unique physicochemical properties in many applications. Here we demonstrate the synthesis and study the stability of Cu_3Au intermetallic nanowires. The synthesis is achieved by using Cu@Au core−shell nanowires as precursors. With appropriate Cu/Au stoichiometry, the Cu@Au core−shell nanowires are transformed into fully ordered Cu_3Au nanowires under thermal annealing. Thermally-driven atom diffusion accounts for this transformation as revealed by X-ray diffraction and electron microscopy studies. The twin boundaries abundant in the Cu@Au core−shell nanowires facilitate the ordering process. The resulting Cu_3Au intermetallic nanowires have uniform and accurate atomic positioning in the crystal lattice, which enhances the nobility of Cu. No obvious copper oxides are observed in fully ordered Cu_3Au nanowires after annealing in air at 200 °C, a temperature that is much higher than those observed in Cu@Au core−shell and pure Cu nanowires. This work opens up an opportunity for further research into the development and applications of intermetallic nanowires.

Introduction

Multimetallic nanocrystals have applications in catalysis, sensors, electronics, and plasmonics [1−3]. The atomic posi- tioning of each metal component in the nanocrystals offers an effective way to tune their physical and chemical properties [4−6]. The most common solid mixtures include solid solutions, intermetallic compounds, and heterostructures. Among the three, intermetallic compounds are characterized by defined stoichiometry and ordered atomic arrangement. The highly ordered atomic positioning in intermetallic compounds gives rise to geometric and electronic homogeneity. Moreover, intermetallics generally exhibit improved stability against oxidation and etching than the random alloy counterparts with identical composition [7, 8]. The enhanced stabilities are attributed to either their more negative enthalpy of formation, or the existence of noble metal overlayers [9, 10].

Although intermetallic compounds are thermodynamically more stable than solid solutions below the order-disorder transition temperatures (T_C), wet-chemical synthesis commonly yields random alloys because of the relatively high kinetic barriers of ordering. Thermal annealing has been proven an effective way to convert preformed nanocrystals into intermetallics [11−13]. However, during the thermal treatment, the nanocrystals tend to evolve into spherical particles [14], and grow larger via agglomeration and Ostwald ripening. Protective shells (MgO, SiO_2, and polydopamine) were therefore employed to mitigate particle sintering [15−17]. Uniform intermetallic nanoparticles with reduced particle sizes (sub-10 nm) have been made using this encapsulation approach [18, 19]. Despite the progress in size control, shape control of intermetallic nanocrystals remains a formidable task. The morphologies of the preformed nanocrystals can hardly maintain during thermal annealing due to accelerated surface diffusion at elevated temperatures [14, 20]. So far, only a few intermetallic nanocrystals have been achieved with well-defined shapes, including Pt−Sn, Pt−Pb, Pt−Bi, Pd−Sn, and Pd−Cu [21−28]. Here, we demonstrate a shape- preserving conversion of Cu@Au core−shell nanowires to Cu_3Au intermetallic nanowires.

Results and discussion

The Cu−Au system has been widely used as an ideal system to study the disorder−order phase transformation [29−31]. This is because the Cu−Au system is featured by continuous series of solid solutions, as well as various forms of intermetallic

structures. In order to achieve shape preservation during thermal treatment, it is a necessity to achieve disorder-to- order transition at a lower annealing temperature. One strategy comes to the forefront is to introduce vacancies/defects into the material, which can lower the kinetic barriers of atom diffusion [32, 33]. Therefore, raising the vacancy/defect concentration will greatly facilitate the ordering process [10, 34].

In this regard, we chose defective and highly strained Cu nanowires as the starting material for the synthesis of Cu_3Au intermetallic nanowires. The Cu nanowires were prepared using a free radical approach developed by our group (Fig. S1(a) in the Electronic Supplementary Material (ESM)) [35]. The five-fold twinned structure of Cu nanowires is well documented [35−38]. Each wire can be considered to consist of five single-crystalline grains separated by five twin planes (i.e. planar defects) aligned along the wire axis. The gaps between the adjacent grains (inset in Fig. S1(b) in the ESM) can give rise to lattice strains and distortions, as reflected in the X-ray diffraction (XRD) which presents perceptible peak asymmetry and peak splitting (Fig. S1(b) in the ESM, blue line) [39, 40]. As a reference, single-crystalline Cu nanocubes exhibited reflections with highly symmetric shapes (Fig. S1(b) in the ESM, red line). We reasoned that the existence of these planar defects in nanowire would help the subsequent disorder−order transition. An appropriate amount of Au was then coated on the as-made Cu nanowires to reach a stoichiometric composition close to Cu_3Au, through epitaxial deposition following the procedure reported previously [41]. It should be noted that the Au deposition was conducted at a temperature (130 °C) lower than the synthetic temperature (165 °C) of the parent Cu nanowires (see Experimental section). Therefore, it is reasonable to assume that the internal lattice defects near the twin planes were kept in the resultant Cu@Au core−shell nanowires. The as-made Cu@Au core−shell nanowires had an average diameter of 22 ± 5 nm (Figs. S2(a) and S2(b) in the ESM). Between the shell and the core could be observed clear and even interface (Figs. S2(b) and S2(c) in the ESM), where the atomic diffusion would occur.

To make Cu_3Au intermetallic nanowires, the as-synthesized Cu@Au core−shell nanowires were subjected to thermal annealing under forming gas (10% H_2/Ar). Figure 1(a) and Fig. S3 in the ESM present the evolution of XRD patterns of Cu@Au core−shell nanowires after being annealed at progressively increased temperatures, with a duration of one hour for each.

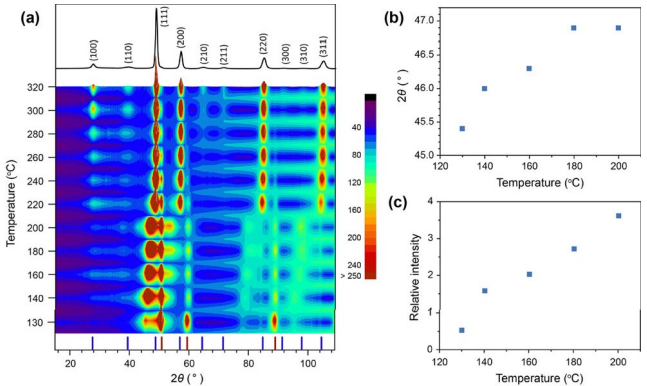

Figure 1 (a) Contour surface of the XRD evolution of Cu@Au core− shell nanowires after annealing at temperatures from 140 to 320 °C. Blue and red lines represent the reference reflections of $L1_2$ Cu_3Au (JCPDS#65-9737) and Cu (JCPDS#65-9026), respectively. (b) The two-theta value of the A1 Cu−Au(111) reflection as a function of the annealing temperature. (c) The temperature-dependence of the integral intensity of the A1 Cu−Au(111) reflection in relative to that of Cu(111) reflection.

In general, there are three distinct stages that can be recognized from the XRD evolution: below 200 °C, from 200 to 220 °C, and above 220 °C. Specifically, the pristine Cu@Au core−shell nanowires exhibited major peaks similar to face- centered cubic (fcc) Cu. A hump showed up between the Cu(111) and Au(111) diffractions, suggesting partial mixing of Au and Cu in the vicinity of core/shell interface. The hump evolved into a broad peak after annealing at 140 °C, positioning at a 2θ value of 46°. It can be assigned to the reflection of A1 Cu−Au(111). Further increasing the annealing temperature from 160 to 200 °C, the A1 Cu−Au(111) reflection slightly shifted toward higher 2θ values (Fig. 1(b)) and its integral intensity dramatically increased in relative to that of Cu(111) (Fig. 1(c)). These observations indicate a higher degree of mixing between Au and Cu upon thermal treatment. Meanwhile, weak superlattice reflections (100 and 110) began to appear when the annealing temperature was above 160 °C. Tetragonal intermetallic CuAu ($L1_0$ phase) mixed with Cu could be identified in the sample after annealing at both 180 and 200 °C (Fig. 1(a) and Fig. S3 in the ESM). These results suggest that the phase transition temperature was reduced for the five-fold twinned nanowires as compared with the bulk CuAu (ca. 235−310 °C [42]). While the XRD patterns followed a gradual evolution below 200 °C, a drastic change took place when elevating the annealing temperature to 220 °C. A new set of reflections, which could be assigned to cubic intermetallic Cu_3Au ($L1_2$ phase), suddenly showed up in replacement of tetragonal CuAu phase. This transformation was accompanied by the consumption of Cu phase, as reflected by the largely reduced peak intensities of Cu(111) and Cu(200). Thereafter, with the proceeding of atomic diffusion at even higher temperatures (≥ 240 °C), more and more residual Cu was incorporated into the lattice of $L1_2$ phase of Cu_3Au until a complete transformation accomplished at 320 °C. The one-dimensional morphology was well preserved in the final products (Fig. S4 in the ESM).

It is conceivable that a diffusion layer would form around the Cu/Au interface in response to thermal annealing. The diffusion layer can be considered as an interface joint between co-existing phases. It would provide a venue for the mixing and ordering of Cu and Au atoms. This hypothesis is substantiated by elemental mappings using energy dispersive X-ray spectroscopy (EDS). As depicted in Fig. 2(a), the initial Cu@Au core−shell nanowire had Cu (green) uniformly coated by a conformal shell of Au (red). The compositional line-scan profile across the wire also suggests a core−shell configuration of the two elements. There was appreciable change in the elemental distribution after annealing at 200 °C (Fig. 2(b)). Au was no longer enriched on the surface of Cu wire, but spread inward

Figure 2 HAADF-STEM images, EDS elemental mappings, and line- scan profiles (bottom panels) of a pristine Cu@Au core−shell nanowire (a), an intermediate obtained after annealing at 200 °C (b), and a product obtained after annealing at 320 °C (c). Green and red colors represent Cu and Au, respectively.

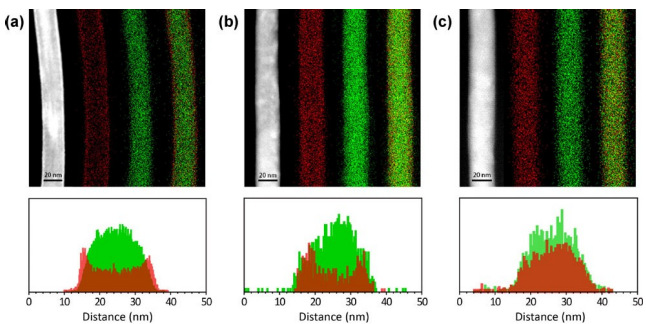

instead. The corresponding line-scan profile

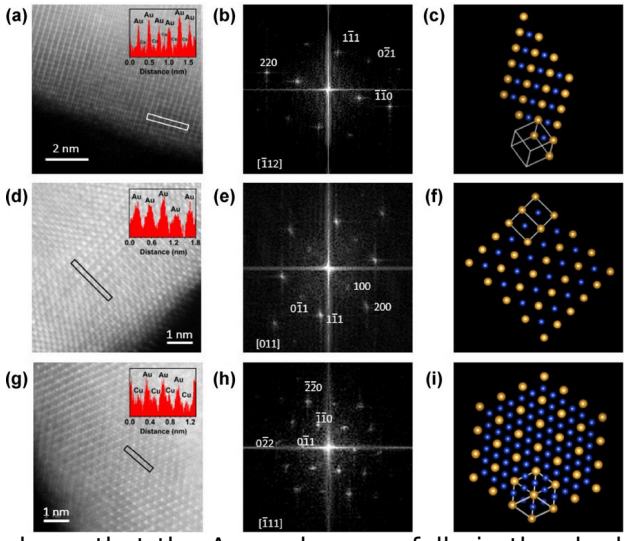

shows that the Au peaks were fully in the shade of the Cu signals, indicative of the diffusion and mixing of the two elements from the outer shell. Figure 2(c) shows the elemental mapping of the final $L1_2$ Cu_3Au nanowire, wherein the Cu and Au were homo- geneously distributed, very different from the initial core−shell arrangement.

The atomic arrangement in the $L1_2$ Cu_3Au nanowire was further investigated using aberration-corrected high-angle annular dark-field (HAADF) scanning transmission electron microscopy (STEM). Figure 3 shows the atomic-resolution imag es of the $L1_2$ Cu_3A u viewed along three differ ent orientations, i.e. [112], [011], and [111], respectively. Because the contrast in HAADF-STEM image is proportional to the square of atomic number (Z), Au atom columns have higher intensity than Cu in the images. The periodic oscillations of bright (Au) and dark (Cu) columns directly reflect the ordered lattice in the $L1_2$ Cu_3Au nanowire. The intensity profiles measured across the nanowire are given in the insets in Fig. 3. The projected atomic arrangements along different zone axes (Figs. 3(c), 3(f), and 3(i)) exhibit oblique, rectangular, hexagonal lattices, respectively. These results clearly indicate the highly ordered structure of the resultant Cu_3Au nanowire.

We noticed that wire sintering was not completely suppressed under the forming gas annealing if the wires were too close to each other on the substrate. As highlighted in Fig. S4 in the ESM, a bunch of wires melted together after the thermal treatment at 320 °C. More benign annealing conditions are desired to address this problem. Since $L1_2$ Cu_3Au was already observed at 220 °C (Fig. 1(a)), we attempted to convert Cu@Au core−shell nanowires into intermetallics at 220 °C with prolonged annealing treatment. Figure S5 in the ESM shows the time-dependent XRD patterns. In general, extending the duration of thermal treatment did make the $L1_2$ Cu_3Au phase more dominant in the products, although a very weak Cu(111) reflection still remained. This is probably because the diffusion of remaining Cu needs to cross a longer distance. Alternatively, we also carried out thermal treatment in high boiling-point solvent (1-octadecene). We expected that a high coverage of capping agents (oleylamine and oleic acid) on the

Figure 3 Aberration-corrected HAADF-STEM images ((a), (d), (g)), corresponding f ast Fourier transf orms ((b), (e), (h)), and projected unit cells along the [112], [011], and [111] axes ((c), (f), (i)) of the $L1_2$ Cu_3Au intermetalic nanowires. Blue and yellow spheres represent Cu and Au atoms, respectively.

surface of nanowires would keep them from sinter. Indeed, the resultant Cu_3Au intermetallic nanowires were better dispersed than those made by forming gas annealing, but the length of the nanowires became relatively short (Fig. S6 in the ESM).

Cu–Au intermetallic compounds have shown great promise in applications regarding catalysis, coating, and electronic devices [43−45]. In particular, the electrical resistivity of $L1_2$ Cu_3Au is comparable to that of the highly conductive Cu [46, 47], making the $L1_2$ Cu_3Au nanowires a potential candidate for transparent conductive materials. Previously, we demonstrated that Cu@Au core–shell nanowires were more stable against humidity and air than Cu nanowires [41]. Here, we further compare the stability of Cu, Cu@Au, and $L1_2$ Cu_3Au nanowires under air annealing at temperatures up to 300 °C. No obvious morphological changes were observed in ordered Cu_3Au nanowires until 250 °C, at which the wire surfaces started to become rough (Fig. 4(a)). In contrast, similar structural degradations were observed for Cu@Au and Cu nanowires at much lower temperatures. Pieces of low-contrast flakes appeared on Cu@Au core−shell nanowires at 200 °C, while the surfaces of pure Cu nanowires were no longer smooth and intact at 150 °C. The low-contrast surface species were identified to be copper oxides as revealed by elemental EDS mapping (Fig. S7 in the ESM). The degradation process was then followed using XRD (Figs. 4(b)–4(d) and Fig. S8 in the ESM). The reflections of copper oxides (Cu_2O and/or CuO) began to appear at 250 and 200 oC for ordered Cu_3Au and Cu@Au, respectively, in line with the morphological changes observed in the TEM. However, Cu nanowires already suffered from partial oxidation even at room temperature (RT), as evidenced by the presence of $Cu_2O(111)$ reflection. The intensity of $Cu_2O(111)$ gradually increased with elevated temperatures. It is worth noting that the cuprous oxides all transformed into cupric oxides above 250 °C. These results indicate that the thermal stability under oxidative atmosphere follows the order of $L1_2$ Cu_3Au > Cu@Au core−shell > pure Cu nanowires. The oxidation-resistant property of $L1_2$ Cu_3Au nanowires could be attributed to the enhanced nobility of Cu atoms in the intermetallic lattice [48], where the accurate atomic positioning leads to homogeneity of electronic structures.

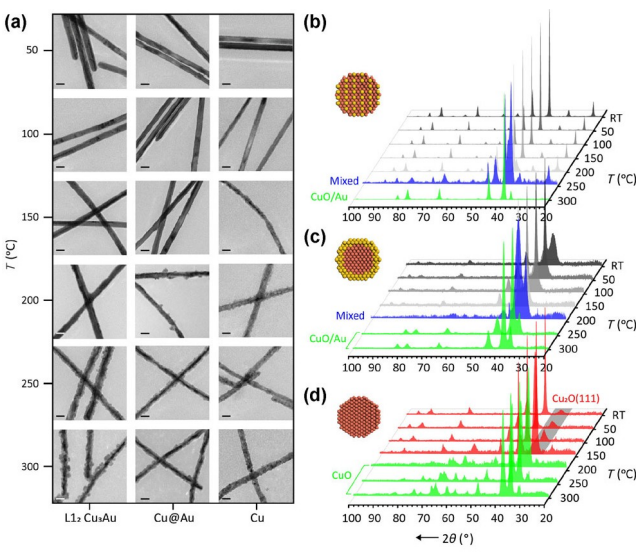

Figure 4 Thermal stability of Cu-based nanowires in air at different tem- peratures. TEM images (a) and XRD patterns (b)–(d) of $L1_2$ Cu_3Au (b), Cu@Au core−shell prepared at 140 °C (c), and Cu nanowires (d) after annealing in air for one hour at elevated temperatures. Scale bar: 20 nm.

Conclusion

In summary, we have shown a shape-controlled transformation of Cu@Au core−shell nanowires into Cu_3Au intermetallic nanowires. The ordering process was initiated at a relatively low temperature (160 °C) probably due to the presence of considerable twin planes in the parent nanowires, which can lower the kinetic barriers for atomic diffusion. During the transformation, $L1_0$ CuAu was identified as an intermediate phase below 200 °C, and a drastic phase transition from $L1_0$ CuAu to $L1_2$ Cu_3Au was observed when increasing the annealing temperature from 200 to 220 oC. The ordered Cu_3Au nanowires have shown enhanced thermal stability in air compared with Cu and Cu@Au core−shell nanowires. Further improvement is needed to retain the high aspect-ratios of the parent Cu@Au nanowires during the thermal annealing, to fulfill the requirement of nanowire-based transparent conductors.

Experimental

1.1 Chemicals

Copper(II) chloride dihydrate ($CuCl_2 \cdot 2H_2O$, 99.999%), chloro(triphenylphosphine)gold(I) ($(Ph_3P)AuCl$, ≥ 99.9%), tris(trimethylsilyl)silane (TTMSS, 97%), trioctylphosphine (90%), 1-octadecene (90%), oleylamine (70%), and oleic acid (90%) were purchased from Sigma-Aldrich. Toluene (≥ 99.9%) was purchased from Fisher Scientific. All chemicals were used as received without further purification.

1.2 Characterizations

TEM was acquired by Hitachi H-7650. HAADF-STEM and EDS mapping were performed with FEI TitanX 60-300. High-resolution HAADF-STEM was measured by JEOL double aberration-corrected GrandARM microscope. XRD was carried out using Bruker D-8 General Area Detector Diffraction System (GADDS) with Co Kα source and Bruker AXS D8 Advance diffractometer with Cu Kα source.

1.3 Synthesis of Cu nanowires

In a typical synthesis, 85 mg of $CuCl_2 \cdot 2H_2O$ (0.5 mmol) and

0.5 g of oleylamine were mixed in a Schlenk flask. The copper precursor was dissolved at 70 °C under stirring. The mixture was degassed for 30 min, followed by N_2 purging. Then, 0.5 g of tris(trimethylsily)silane (2 mmol) was added into the flask. The resultant blue solution was slowly heated up to 110 °C in an oil bath. When the color of the solution turned into clear yellow, the temperature of the oil bath was further increased to 165 °C. The reaction was left at this temperature for 16 h for the growth of Cu nanowires.

4.4 Synthesis of Cu@Au nanowires

Right after the growth of the Cu nanowires, the reaction flask was placed in an oil bath preheated at 130 or 140 °C. The as-synthesized Cu nanowires were kept in the growth solution under N_2 protection. $(Ph_3P)AuCl$ (80 mg) dissolved in trioctylphosphine (1 mL) was injected into the flask using syringe. The reaction was maintained at this temperature for 1 h before cooling down to room temperature. The products were washed with toluene and collected by centrifugation at 8,000 rpm.

4.5 Transformation into Cu_3Au intermetallic nanowires (solid-state)

The collected Cu@Au core−shell nanowires were re-dispersed

in toluene and drop-casted on glass slides. The samples were annealed in a hydrogen/argon mixture (H_2/Ar:10/90) at different temperatures for one hour. After cooling down, the samples were stored in N_2 box for further characterizations.

4.6 Transformation into Cu_3Au intermetallic nanowires (liquid-phase)

The collected Cu@Au core−shell nanowires were re-dispersed in 6 mL of 1-octadecene, 0.2 mL of oleylamine, and 0.2 mL of oleic acid in a Schlenk flask. The mixture was degassed at 80 °C for 30 min followed by inert gas purging. Then, the flask was placed into a salt bath preheated at 335 °C and kept for 70 min under stirring at 60 rpm. After cooling down to room temperature, the products were washed with toluene and collected by centrifugation at 8,000 rpm.

4.7 Thermal annealing in air

The Cu-based nanowires were re-dispersed in toluene and loaded on proper substrates, such as Ni grids for TEM and glass slides for XRD. The muffle furnace was pre-heated at designated temperatures before the samples were put into it. The samples were taken out after one-hour thermal treatment in air, and stored in N_2 box for further characterizations.

Acknowledgements

This work was financially supported by BASF Corporation (Award Number 53093). Work at the National Center for Electron Microscopy (NCEM), the Molecular Foundry was supported by the Director, Office of Science, Office of Basic Energy Sciences, of the U.S. Department of Energy under Contract No. DE-AC02-05CH11231. Aberration-corrected STEM was supported by the Center for high-resolution Electron Microscopy (CħEM) at ShanghaiTech University.
T. L. acknowledges fellowship from Suzhou Industrial Park. We acknowledge P. Alivisatos for access to the Bruker D-8 Diffractometer for XRD analysis.

Electronic Supplementary Material: Supplementary material (additional TEM, HAADF-STEM, EDS mapping images, and XRD patterns of the nanowires) is available in the online version of this article at https://doi.org/10.1007/s12274-020- 2900-z.

References

[1] Chen, P. C.; Liu, X. L.; Hedrick, J. L.; Xie, Z.; Wang, S. Z.; Lin, Q. Y.; Hersam, M. C.; Dravid, V. P.; Mirkin, C. A. Polyelemental nanoparticle libraries. *Science* **2016**, *352*, 1565–1569.
[2] Yao, Y. G.; Huang, Z. N.; Xie, P. F.; Lacey, S. D.; Jacob, R. J.; Xie, H.; Chen, F. J.; Nie, A. M.; Pu, T. C.; Rehwoldt, M. et al. Carbothermal shock synthesis of high-entropy-alloy nanoparticles. *Science* **2018**, *359*, 1489–1494.
[3] Cortie, M. B.; McDonagh, A. M. Synthesis and optical properties of hybrid and alloy plasmonic nanoparticles. *Chem*. *Rev*. **2011**, *111*, 3713–3735.
[4] Casado-Rivera, E.; Volpe, D. J.; Alden, L.; Lind, C.; Downie, C.; Vázquez-Alvarez, T.; Angelo, A. C. D.; DiSalvo, F. J.; Abruna, H. D. Electrocatalytic activity of ordered intermetallic phases for fuel cell applications. *J. Am*. *Chem*. *Soc*. **2004**, *126*, 4043–4049.
[5] Niu, Z. Q.; Becknell, N.; Yu, Y.; Kim, D.; Chen, C.; Kornienko, N.; Somorjai, G. A.; Yang, P. D. Anisotropic phase segregation and migration of Pt in nanocrystals en route to nanoframe catalysts. *Nat*. *Mater*. **2016**, *15*, 1188–1194.
[6] Chen, C.; Kang, Y. J.; Huo, Z. Y.; Zhu, Z. W.; Huang, W. Y.; Xin, H. L.; Snyder, J. D.; Li, D. G.; Herron, J. A.; Mavrikakis, M. et al. Highly crystalline multimetallic nanoframes with three-dimensional

electrocatalytic surfaces. *Science* **2014**, *343*, 1339–1343.

[7] Rößner, L.; Armbrüster, M. Electrochemical energy conversion on intermetallic compounds: A review. *ACS Catal*. **2019**, *9*, 2018– 2062.

[8] Escudero-Escribano, M.; Verdaguer-Casadevall, A.; Malacrida, P.; Grønbjerg, U.; Knudsen, B. P.; Jepsen, A. K.; Rossmeisl, J.; Stephens, I. E. L.; Chorkendorff, I. Pt_5Gd as a highly active and stable catalyst for oxygen electroreduction. *J. Am. Chem. Soc.* **2012**, *134*, 16476–16479.

[9] Wang, D. L.; Xin, H. L.; Hovden, R.; Wang, H. S.; Yu, Y. C.; Muller, D. A.; DiSalvo, F. J.; Abruña, H. D. Structurally ordered intermetallic platinum–cobalt core–shell nanoparticles with enhanced activity and stability as oxygen reduction electrocatalysts. *Nat. Mater.* **2013**, *12*, 81–87.

[10] Yan, Y. C.; Du, J. S.; Gilroy, K. D.; Yang, D. R.; Xia, Y. N.; Zhang, H. Intermetallic nanocrystals: Syntheses and catalytic applications. *Adv. Mater.* **2017**, *29*, 1605997.

[11] Xiong, Y.; Yang, Y.; DiSalvo, F. J.; Abruña, H. D. Pt-decorated composition-tunable Pd–Fe@Pd/C core–shell nanoparticles with enhanced electrocatalytic activity towards the oxygen reduction reaction. *J. Am. Chem. Soc.* **2018**, *140*, 7248–7255.

[12] Bauer, J. C.; Chen, X. L.; Liu, Q. S.; Phan, T. H.; Schaak, R. E. Converting nanocrystalline metals into alloys and intermetallic compounds for applications in catalysis. *J. Mater. Chem.* **2008**, *18*, 275–282.

[13] Wang, C. Y.; Chen, D. P.; Sang, X. H.; Unocic, R. R.; Skrabalak, S. E. Size-dependent disorder–order transformation in the synthesis of monodisperse intermetallic PdCu nanocatalysts. *ACS Nano* **2016**, *10*, 6345–6353.

[14] Lu, N.; Wang, J. G.; Xie, S. F.; Xia, Y. N.; Kim, M. J. Enhanced shape stability of Pd–Rh core–frame nanocubes at elevated temperature: *In situ* heating transmission electron microscopy. *Chem. Commun.* **2013**, *49*, 11806–11808.

[15] Li, J. R.; Xi, Z.; Pan, Y. T.; Spendelow, J. S.; Duchesne, P. N.; Su, D.; Li, Q.; Yu, C.; Yin, Z. Y.; Shen, B. et al. Fe stabilization by intermetallic L1 -FePt and Pt catalysis enhancement in $L1_0$-FePt/Pt_0 nanoparticles for efficient oxygen reduction reaction in fuel cells. *J. Am. Chem. Soc.* **2018**, *140*, 2926–2932.

[16] Maligal-Ganesh, R. V.; Xiao, C. X.; Goh, T. W.; Wang, L. L.; Gustafson, J.; Pei, Y. C.; Qi, Z. Y.; Johnson, D. D.; Zhang, S. R.; Tao, F. et al. A ship-in-a-bottle strategy to synthesize encapsulated intermetallic nanoparticle catalysts: Exemplified for furfural hydrogenation. *ACS Catal*. **2016**, *6*, 1754–1763.

[17] Chung, D. Y.; Jun, S. W.; Yoon, G.; Kwon, S. G.; Shin, D. Y.; Seo, P.; Yoo, J. M.; Shin, H.; Chung, Y. H.; Kim, H. et al. Highly durable and active PtFe nanocatalyst for electrochemical oxygen reduction reaction. *J. Am. Chem. Soc.* **2015**, *137*, 15478–15485.

[18] Liang, J. S.; Li, N.; Zhao, Z. L.; Ma, L.; Wang, X. M.; Li, S. Z.; Liu, X.; Wang, T. Y.; Du, Y. P.; Lu, G. et al. Tungsten-doped $L1_0$-PtCo ultrasmall nanoparticles as a high-performance fuel cell cathode. *Angew. Chem.* **2019**, *131*, 15617–15623.

[19] Wang, T. Y.; Liang, J. S.; Zhao, Z. L.; Li, S. Z.; Lu, G.; Xia, Z. C.; Wang, C.; Luo, J. H.; Han, J. T.; Ma, C. et al. Sub-6 nm fully ordered $L1_0$-Pt–Ni–Co nanoparticles enhance oxygen reduction via Co doping induced ferromagnetism enhancement and optimized surface strain. *Adv. Energy Mater.* **2019**, *9*, 1803771.

[20] Wang, C.; Hou, Y. L.; Kim, J.; Sun, S. H. A general strategy for synthesizing FePt nanowires and nanorods. *Angew. Chem., Int. Ed.* **2007**, *46*, 6333–6335.

[21] Bu, L. Z.; Zhang, N.; Guo, S. J.; Zhang, X.; Li, J.; Yao, J. L.; Wu, T.; Lu, G.; Ma, J. Y.; Su, D. et al. Biaxially strained PtPb/Pt core/shell nanoplate boosts oxygen reduction catalysis. *Science* **2016**, *354*, 1410–1414.

[22] Chen, Q. L.; Zhang, J. W.; Jia, Y. Y.; Jiang, Z. Y.; Xie, Z. X.; Zheng, L. S. Wet chemical synthesis of intermetallic Pt_3Zn nanocrystals via weak reduction reaction together with UPD process and their excellent electrocatalytic performances. *Nanoscale* **2014**, *6*, 7019– 7024.

[23] Chou, N. H.; Schaak, R. E. Shape-controlled conversion of *β*-Sn nanocrystals into intermetallic *M*-Sn (*M* = Fe, Co, Ni, Pd) nano- crystals. *J. Am. Chem. Soc.* **2007**, *129*, 7339–7345.

[24] Gao, Q.; Ju, Y. M.; An, D.; Gao, M. R.; Cui, C. H.; Liu, J. W.; Cong, H. P.; Yu, S. H. Shape-controlled synthesis of monodisperse PdCu nanocubes and their electrocatalytic Properties. *ChemSusChem* **2013**, *6*, 1878–1882.

[25] Liao, H. B.; Zhu, J. H.; Hou, Y. L. Synthesis and electrocatalytic properties of PtBi nanoplatelets and PdBi nanowires. *Nanoscale* **2014**, *6*, 1049–1055.

[26] Luo, Z. S.; Lu, J. M.; Flox, C.; Nafria, R.; Genç, A.; Arbiol, J.; Llorca, J.; Ibáñez, M.; Morante, J. R.; Cabot, A. Pd_2Sn [010] nanorods as a highly active and stable ethanol oxidation catalyst. *J. Mater. Chem. A* **2016**, *4*, 16706–16713.

[27] Maksimuk, S.; Yang, S. C.; Peng, Z. M.; Yang, H. Synthesis and characterization of ordered intermetallic PtPb nanorods. *J. Am. Chem. Soc.* **2007**, *129*, 8684–8685.

[28] Rong, H. P.; Mao, J. J.; Xin, P. Y.; He, D. S.; Chen, Y. J.; Wang, D. S.; Niu, Z. Q.; Wu, Y. E.; Li, Y. D. Kinetically controlling surface structure to construct defect-rich intermetallic nanocrystals: Effective and stable catalysts. *Adv. Mater.* **2016**, *28*, 2540–2546.

[29] Liu, S. J.; Sun, Z. H.; Liu, Q. H.; Wu, L. H.; Huang, Y. Y.; Yao, T.; Zhang, J.; Hu, T. D.; Ge, M. R.; Hu, F. C. et al. Unidirectional thermal diffusion in bimetallic Cu@Au nanoparticles. *ACS Nano* **2014**, *8*, 1886–1892.

[30] Sra, A. K.; Ewers, T. D.; Schaak, R. E. Direct solution synthesis of intermetallic AuCu and $AuCu_3$ nanocrystals and nanowire networks. *Chem. Mater.* **2005**, *17*, 758–766.

[31] Yang, J. H.; Chng, L. L.; Yang, X. F.; Chen, X. J.; Ying, J. Y. Multiply- twinned intermetallic AuCu pentagonal nanorods. *Chem. Commun.* **2014**, *50*, 1141–1143.

[32] Barth, S.; Boland, J. J.; Holmes, J. D. Defect transfer from nanoparticles to nanowires. *Nano Lett.* **2011**, *11*, 1550–1555.

[33] Li, Q.; Wu, L. H.; Wu, G.; Su, D.; Lv, H. F.; Zhang, S.; Zhu, W. L.; Casimir, A.; Zhu, H. Y.; Mendoza-Garcia, A. et al. New approach to fully ordered fct-FePt nanoparticles for much enhanced electrocatalysis in acid. *Nano Lett.* **2015**, *15*, 2468–2473.

[34] Li, J. R.; Sun, S. H. Intermetallic nanoparticles: Synthetic control and their enhanced electrocatalysis. *Acc. Chem. Res.* **2019**, *52*, 2015–2025.

[35] Cui, F.; Yu, Y.; Dou, L. T.; Sun, J. W.; Yang, Q.; Schildknecht, C.; Schierle-Arndt, K.; Yang, P. D. Synthesis of ultrathin copper nanowires using tris(trimethylsilyl)silane for high-performance and low-haze transparent conductors. *Nano Lett*. **2015**, *15*, 7610–7615.
[36] Jin, M. S.; He, G. N.; Zhang, H.; Zeng, J.; Xie, Z. X.; Xia, Y. N. Shape—controlled synthesis of copper nanocrystals in an aqueous solution with glucose as a reducing agent and hexadecylamine as a capping agent. *Angew*. *Chem., Int*. *Ed*. **2011**, *50*, 10560–10564.
[37] Yang, H. J.; He, S. Y.; Tuan, H. Y. Self-seeded growth of five-fold twinned copper nanowires: Mechanistic study, characterization, and SERS applications. *Langmuir* **2014**, *30*, 602–610.
[38] Cui, F.; Dou, L. T.; Yang, Q.; Yu, Y.; Niu, Z. Q.; Sun, Y. C.; Liu, H.; Dehestani, A.; Schierle-Arndt, K.; Yang, P. D. Benzoin radicals as reducing agent for synthesizing ultrathin copper nanowires. *J*. *Am*. *Chem*. *Soc*. **2017**, *139*, 3027–3032.
[39] Niu, Z. Q.; Cui, F.; Kuttner, E.; Xie, C. L.; Chen, H.; Sun, Y. C.; Dehestani, A.; Schierle-Arndt, K.; Yang, P. D. Synthesis of silver nanowires with reduced diameters using benzoin-derived radicals to make transparent conductors with high transparency and low haze. *Nano Lett*. **2018**, *18*, 5329–5334.
[40] Sun, Y. G.; Ren, Y.; Liu, Y. Z.; Wen, J. G.; Okasinski, J. S.; Miller, D.
J. Ambient-stable tetragonal phase in silver nanostructures. *Nat*. *Commun*. **2012**, *3*, 971.
[41] Niu, Z. Q.; Cui, F.; Yu, Y.; Becknell, N.; Sun, Y. C.; Khanarian, G.; Kim, D.; Dou, L. T.; Dehestani, A.; Schierle-Arndt, K. et al. Ultrathin epitaxial Cu@Au core-shell nanowires for stable transparent conductors. *J*. *Am*. *Chem*. *Soc*. **2017**, *139*, 7348–7354.
[42] Bonneaux, J.; Guymont, M. Study of the order-disorder transition series in AuCu by in-situ temperature electron microscopy. *Intermetallics* **1999**, *7*, 797–805.
[43] Chen, H. Q.; Nishijima, M.; Wang, G. L.; Khene, S.; Zhu, M. Q.; Deng, X.; Zhang, X. M.; Wen, W.; Luo, Y.; He, Q. G. The ordered and disordered nano-intermetallic AuCu/C catalysts for the oxygen reduction reaction: The differences of the electrochemical performance. *J*. *Electrochem*. *Soc*. **2017**, *164*, F1654–F1661.

[44] Kim, D.; Xie, C. L.; Becknell, N.; Yu, Y.; Karamad, M.; Chan, K.; Crumlin, E. J.; Nørskov, J. K.; Yang, P. D. Electrochemical activation of CO_2 through atomic ordering transformations of AuCu nanoparticles. *J. Am. Chem. Soc.* **2017**, *139*, 8329–8336.

[45] Tee, S. Y.; Ye, E. Y.; Pan, P. H.; Lee, C. J. J.; Hui, H. K.; Zhang, S. Y.; Koh, L. D.; Dong, Z. L.; Han, M. Y. Fabrication of bimetallic Cu/Au nanotubes and their sensitive, selective, reproducible and reusable electrochemical sensing of glucose. *Nanoscale* **2015**, *7*, 11190–11198.

[46] Jacobsson, P.; Sundqvist, B. Pressure dependence of the thermal and electrical conductivities of the intermetallic compounds AuCu and $AuCu_3$. *J. Phys. Chem. Solids* **1988**, *49*, 441–450.

[47] Johansson, C. H.; Linde, J. O. Röntgenographische und elektrische Untersuchungen des CuAu-Systems. *Annalen der Physik* **1936**, *417*, 1–48.

[48] Parks, B. W. Jr.; Fritz, J. D.; Pickering, H. W. The difference in the electrochemical behavior of the ordered and disordered phases of Cu_3Au. *Scr. Metall.* **1989**, *23*, 951–956.